Journal of Global Positioning Systems (*2022*)
Vol. 18, No. 1: 15-27
DOI: 10.5081/jgps.18.1.15

Journal of Global Positioning Systems
2022
© CPGPS

Estimation and analysis of BDS-3 multi-frequency differential code bias using MGEX observations

Haijun Yuan, Zhuoming Hu, Xiufeng He(✉) and Zhetao Zhang
School of Earth Sciences and Engineering, Hohai University, Nanjing 211100, China
✉ **Corresponding author:** Xiufeng He, xfhe@hhu.edu.cn

Abstract: Differential code bias (DCB) significantly affects the ionosphere modeling, precise positioning, and navigation applications when using code observations. With the fully completed BeiDou navigation satellite system (BDS-3), there exist various DCBs of new frequencies and types which should be handled. However, limited types of DCB products for BDS-3 are provided by the analysis institutions (e.g., Chinese Academy of Science (CAS) and German Aerospace Center (DLR)). Hence, for some DCB corrections of new frequencies, they are generally generated by complex linear combinations, which are not friendly to users and may degrade the accuracy. In this study, the estimation method of DCB for BDS-3 is introduced first. Then, the BDS-3 observations from 40 globally distributed stations are selected to estimate the DCBs, including 19 types of DCBs of new frequencies for BDS-3. Moreover, the estimated DCBs are carefully analyzed in terms of inner consistency, external consistency, and stability. For the results of inner consistency, most closure error series are within 0.2 ns, and the closure error series of each satellite fluctuate near zero and have no obvious systematic deviations. For the results of external consistency, the mean deviations of estimated DCBs of each satellite are mainly within 0.3 ns and 0.2 ns for the common types of DCB products of CAS and DLR, respectively. For the results of stability, the mean values of monthly STDs for the estimated DCBs are all smaller than 0.12 ns, which exhibits good stability. The STDs of the directly estimated DCBs are generally smaller than that of the DCB combinations of DLR and CAS. In this sense, the directly estimated DCBs for BDS-3 exhibits good performance in terms of accuracy and stability in this study, which can further provide the DCB corrections for precise positioning and navigation applications.

Keywords: GNSS; BDS-3; multi-frequency; differential code bias; MGEX

1. Introduction

Differential code bias (DCB) physically is defined as the difference in time delays between two different types of code observations. It includes intra-frequency DCB (e.g., C1W-C1C DCB) and inter-frequency DCB (e.g., C1W-C2W DCB) at the satellite or receiver side [1–3]. The DCB not only significantly affects the ionosphere modeling [4,5], but also is the error source in precise positioning, navigation, and timing applications of Global Navigation Satellite System (GNSS) when using code observations [6–8]. Hence, it is of great importance to estimate the DCBs and analyze their property, which can further provide the DCB corrections for GNSS applications.

There exist two major DCB estimation methods depending on the way of ionosphere modeling. The first one is to estimate the DCBs with a global or local ionosphere model simultaneously [9,10]. Another one is to estimate the DCBs after eliminating the ionosphere delays with a prior ionosphere model (e.g., German Aerospace Center (DLR)) [11,12]. The prior ionosphere models generally include the global ionospheric map (GIM) and some broadcast ionospheric models [13]. In addition, the DCBs can also be estimated by modeling the vertical total electron content (VTEC) above each station in the GNSS networks (e.g., Chinese Academy of Science (CAS)) [3,5]. Apart from the estimated DCBs by GNSS observations from ground stations, the estimation of DCBs can rely on the onboard observations from low-earth orbit (LEO) satellites [14–16]. The LEO solutions can achieve comparable and even better stability compared to the ground-based solutions from the global ground GNSS networks [17,18]. The

Editor in charge: Dr. Huizhong Zhu

aforementioned methods and observation sources for DCB estimation are used to obtain the DCB products of Global Positioning System (GPS) and BeiDou Satellite Navigation System (BDS) in recent years [19–21].

Currently, the construction of BDS-3 was fully completed with providing global services to GNSS users. However, there exist various DCBs of new frequencies and types which should be handled for BDS-3 [22,23]. At this time, it leads to a new situation with the following problems and limitations. First, some analysis institutions (e.g., DLR and CAS) only provide specific and limited types of DCB for BDS-3, which is not friendly to GNSS users in the situation of many new frequencies and code types. Second, the DCB corrections are usually added to the code observations by linear combinations of different types of DCB products currently. This will degrade the accuracy of DCB corrections, because the value derived from the linear combination cannot fully represent the true value due to various reasons, which may affect the GNSS applications.

To cope with these problems and limitations, there exists an urgent need to estimate the DCBs of new frequencies and code types for BDS-3. Therefore, in this study, the estimation method of DCB for BDS-3 is introduced first. Then, the BDS-3 observations from 40 globally distributed multi-GNSS experiment (MGEX) stations are selected to estimate the DCBs, including 19 types of DCBs of new frequencies for BDS-3. Moreover, the estimated DCBs are carefully analyzed in terms of inner consistency, external consistency, and stability compared to the DCB products provided by CAS and DLR.

2. Estimation method of BDS-3 DCBs

The dual-frequency code observations of arbitrary frequencies can be expressed as follows:

$$\begin{cases} P_{r,i}^s = \rho_r^s + c \cdot (dt_r - dt^s) + T_r^s + I_{r,i}^s + b_{r,i} + b_i^s + \varepsilon_{r,i}^s \\ P_{r,j}^s = \rho_r^s + c \cdot (dt_r - dt^s) + T_r^s + I_{r,j}^s + b_{r,j} + b_j^s + \varepsilon_{r,j}^s \end{cases} \quad (1)$$

where $P_{r,i}^s$ and $P_{r,j}^s$ denote the code observations on frequency i and j, respectively, the superscript s and subscript r denote the satellite and receiver, respectively, ρ_r^s denotes the geometric distance between the satellite and receiver, c is the light speed in vacuum, dt_r and dt^s denote the clock errors of the receiver and satellite, respectively, T_r^s denotes the tropospheric delays, $I_{r,i}^s$ and $I_{r,j}^s$ denote the ionospheric delays on frequency i and j, respectively, $b_{r,i}$ and $b_{r,j}$ denote the receiver time delays on frequency i and j, respectively, b_i^s and b_j^s denote the satellite time delays on frequency i and j, respectively, and $\varepsilon_{r,i}^s$ and $\varepsilon_{r,j}^s$ denote the code noises on frequency i and j, respectively. Based on (1), the code geometry-free (GF) combination on frequency i and j is deduced as follows:

$$P_{r,ij}^s = P_{r,i}^s - P_{r,j}^s = \left(I_{r,i}^s - I_{r,j}^s\right) + \left(b_{r,i} - b_{r,j}\right) + \left(b_i^s - b_j^s\right) + \Delta\varepsilon_{r,ij}^s \quad (2)$$

where $P_{r,ij}^s$ denotes the code GF combination. As the ionospheric delays are frequency dependent, the combined delay can be eliminated when the selected frequencies of GF combination are same. Otherwise, the ionospheric delays can be corrected by the high-precision GIM products and the corresponding mapping function.

The effect of observation noises can be degraded by averaging the results of GF combinations. At this time, the DCB combination of satellite and receiver can be expressed as follows:

$$DCB_{r,ij} + DCB_{ij}^s = \frac{1}{N}\sum_{t=1}^{N}\left(P_{r,i}^s(t) - P_{r,j}^s(t) - 40.28 \cdot \left(\frac{1}{f_i^2} - \frac{1}{f_j^2}\right) \cdot STEC_r^s\right) \quad (3)$$

where $DCB_{r,ij} = b_{r,i} - b_{r,j}$ is the receiver's DCB on frequency i and j, $DCB_{ij}^s = b_i^s - b_j^s$ is the satellite's DCB on frequency i and j, N is the number of epochs over a continuous period, t is the current observation time, f is the frequency of code observations, and $STEC_r^s$ is the slant total electron content (STEC) in TECU. Therefore, the DCB estimation model can be deduced as follows:

$$\boldsymbol{L}_{\text{sum}} = \boldsymbol{F} \cdot \widehat{\boldsymbol{X}}_{\text{DCB}} \quad (4)$$

wherein $\boldsymbol{L}_{\text{sum}}$ is the vector of DCB combination of satellite and receiver, $\boldsymbol{F}$ is the design matrix, and $\widehat{\boldsymbol{X}}_{\text{DCB}}$ is the estimated DCB vector. Specifically, $\boldsymbol{F}$ and $\widehat{\boldsymbol{X}}_{\text{DCB}}$ are given as follows:

$$\begin{cases} \underset{(u1+u2)\times 1}{\widehat{\boldsymbol{X}}_{\text{DCB}}} = \left[\underset{u1\times 1}{\widehat{\boldsymbol{X}}_{s,\text{DCB}}}, \underset{u2\times 1}{\widehat{\boldsymbol{X}}_{r,\text{DCB}}}\right]^{\text{T}} \\ \underset{n\times(u1+u2)}{\boldsymbol{F}} = \left[\underset{n\times u1}{\boldsymbol{A}}, \underset{n\times u2}{\boldsymbol{B}}\right] \end{cases} \quad (5)$$

where $\widehat{\boldsymbol{X}}_{s,\text{DCB}}$ and $\widehat{\boldsymbol{X}}_{r,\text{DCB}}$ are the DCB vector of satellite and receiver, respectively, $\boldsymbol{A}$ and $\boldsymbol{B}$ are the design matrix for satellite and receiver, respectively, and $u1$ and $u2$ are the numbers of satellites and receivers, respectively. The zero-mean constraint for the DCB of all satellites is introduced to separate the DCBs of satellites and receivers, which is as follows:

$$\begin{cases} \boldsymbol{S} \cdot \widehat{\boldsymbol{X}}_{\text{DCB}} = \boldsymbol{0} \\ \underset{1\times(u1+u2)}{\boldsymbol{S}} = \left[\underset{1\times u1}{\boldsymbol{e}}, \underset{1\times u2}{\boldsymbol{0}}\right], \underset{1\times u1}{\boldsymbol{e}} = [1, \cdots, 1] \end{cases} \quad (6)$$

where $\boldsymbol{S}$ is the design matrix of the zero-mean constraint. Then, the DCBs of the satellites and receivers can be estimated simultaneously by the least-square adjustment, which is as follows:

$$\begin{cases} \hat{\boldsymbol{X}}_{\mathrm{DCB}} = (\boldsymbol{N} + \boldsymbol{S}^{\boldsymbol{T}}\boldsymbol{S})^{-1}\boldsymbol{W} \\ \boldsymbol{D}_{\hat{X}\hat{X}} = \sigma_0^2 \cdot (\boldsymbol{N} + \boldsymbol{S}^{\mathrm{T}}\boldsymbol{S})^{-1} \\ \boldsymbol{N} = \boldsymbol{F}^{\mathrm{T}}\boldsymbol{P}\boldsymbol{F}, \boldsymbol{W} = \boldsymbol{F}^{\mathrm{T}}\boldsymbol{P}\boldsymbol{L}_{\mathrm{sum}} \end{cases} \quad (7)$$

where $\boldsymbol{D}_{\hat{X}\hat{X}}$ is the variance matrix of the estimated DCBs, σ_0^2 is the variance of unit weight, and $\boldsymbol{P}$ is the weight matrix.

3. Experiments and analysis

In this section, the data description and processing strategy are given first. Then, the internal consistency, the external consistency, and the stability of the estimated BDS-3 DCBs are carefully analyzed compared to the products of DLR and CAS.

3.1 Data description and processing strategy

The BDS-3 observations from 40 globally distributed MGEX ground stations are selected to estimate the DCBs in this study. The processing period is continuous 30 days from day of the year (DOY) 60 to 89 in 2021. The distribution of the 40 GNSS stations is displayed in Figure 1. In addition, the types of DCBs of new frequencies for BDS-3 are shown in Table 1, as well as the used stations for estimating each type of DCB. It can be found that there exist 19 types of DCBs that need to be estimated, and the numbers of the used stations for each type of DCB are all larger than 14. There exists a realignment problem before comparing the estimated DCBs in this study, and the specific procedure of solving it can refer to [24]. For the processing strategy, the ionospheric delays of the code GF combinations are corrected by the GIM products provided by CODE with an interval of one hour. The cut-off satellite elevation is set to 20°. The minimum continuous observation arc is set as one hour. The least-square estimator is selected, and the weight matrix is determined by the STD of the GF combination series. The flowchart of the DCB estimation is also shown in Figure 2.

Table 1 Type of the DCB of new frequencies for BDS-3 and the corresponding used stations

Type	Number of the used stations
C1P-C2I	22
C1P-C5P	22
C1P-C6I	22
C1X-C5X	17
C1X-C6I	17
C1X-C7Z	14
C1X-C8X	14
C2I-C1X	17
C2I-C5X	18
C2I-C7Z	15
C2I-C8X	15
C5P-C2I	22
C5P-C6I	22
C5X-C6I	15
C5X-C7Z	15
C5X-C8X	15
C6I-C7Z	15
C6I-C8X	15
C7Z-C8X	15

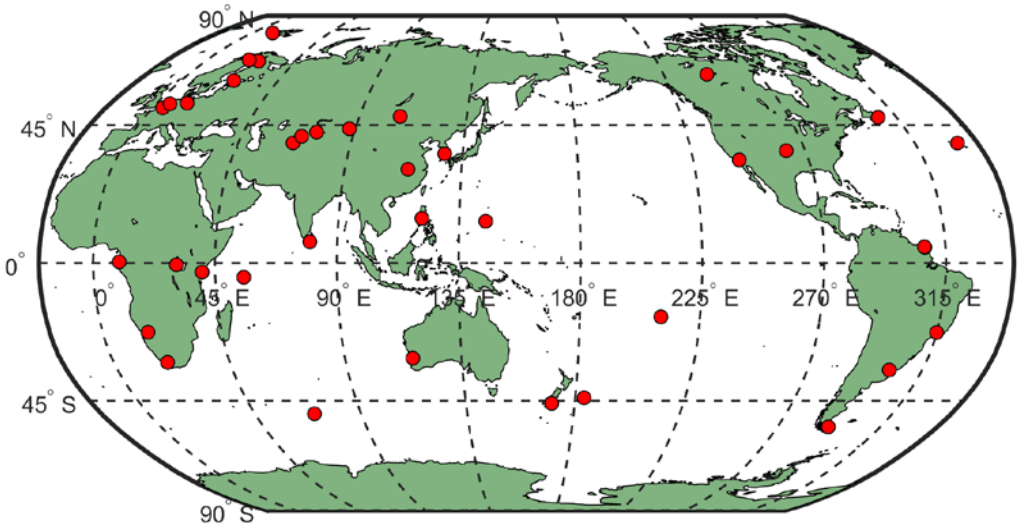

Figure 1 Distribution of the 40 globally distributed MGEX ground stations

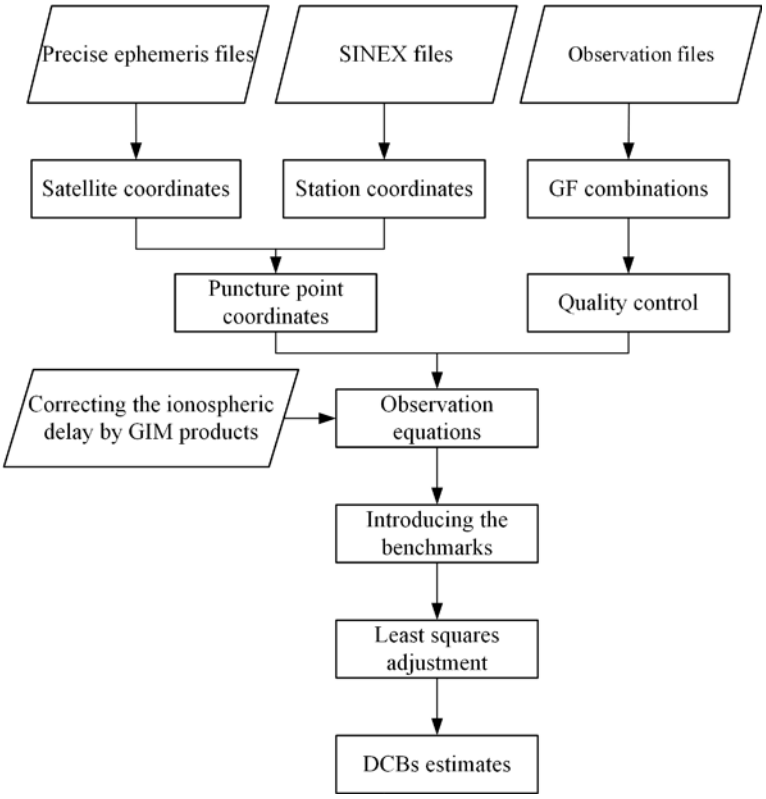

Figure 2 Flowchart of the DCB estimation for BDS-3, where the benchmarks denote the zero-mean constraint condition

3.2 Inner consistency of the estimated BDS-3 DCBs

Theoretically, the closure error for each satellite of these types of DCBs is equal to zero (e.g., $\mathrm{DCB}_{C2I-C5P} - \mathrm{DCB}_{C1P-C2I} - \mathrm{DCB}_{C1P-C5P} = 0$). However, the closure error usually exhibits non-zero in practical estimation due to the effects of observation noises and unmodeled errors. Hence, the property of the closure error can be used to evaluate the inner consistency of these estimated BDS-3 DCBs. For example, the daily closure error series of the estimated DCBs for each satellite are shown in Figures 3 to 6, including the types of C1P-C2I-C5P, C1P-C5P-C6I, C1X-C2I-C5X, and C1X-C5X-C6I. It can be found that most of these closure error series for each satellite are within 0.2 ns, and the closure error series of each satellite fluctuate near zero and have no obvious systematic deviations. In addition, the closure error series of C1P-C2I-C5P and C1P-C5P-C6I are within 0.1 ns, and smaller than that of other types. However, the closure error for some satellites exhibits large on some days (e.g., the closure error of C45 reaches 0.45 ns on DOY 67 and 88 for the type of C1X-C2I-C5X). The reason for this can be attributed to the insufficient number of processing epochs for the satellite on that day.

The mean values and STDs of closure error for the types of C1X-C2I-C5X and C1X-C5X-C6I are further shown in Figures 7 to 8, respectively. As shown in the figures, the mean values of closure error for each satellite are within 0.2 ns, and most of them are within 0.1 ns. In addition, the STDs of closure error for each satellite are within 0.3 ns. Hence, the inner consistency of estimated BDS-3 DCBs in this study exhibits good performance.

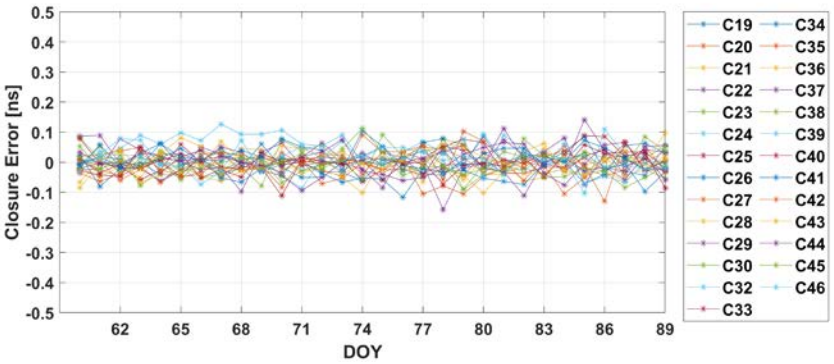

Figure 3 Daily closure error series for the type of C1P-C2I-C5P

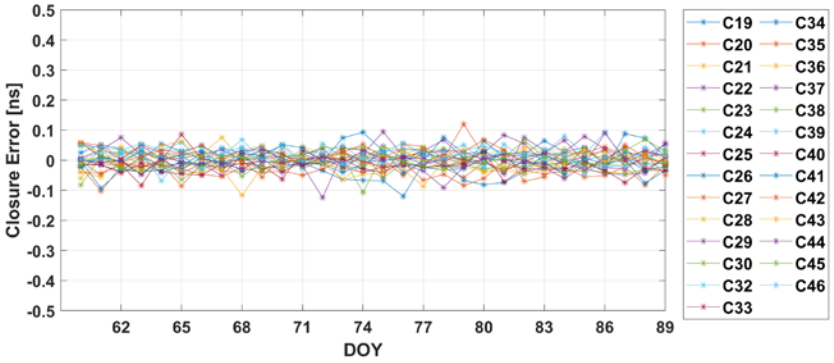

Figure 4 Daily closure error series for the type of C1P-C5P-C6I

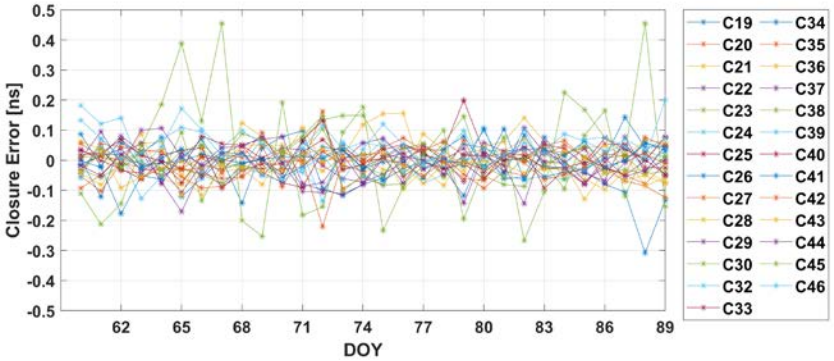

Figure 5 Daily closure error series for the type of C1X-C2I-C5X

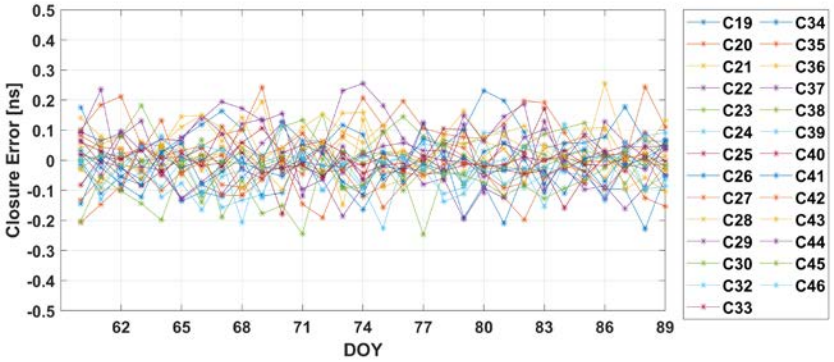

Figure 6 Daily closure error series for the type of C1X-C5X-C6I

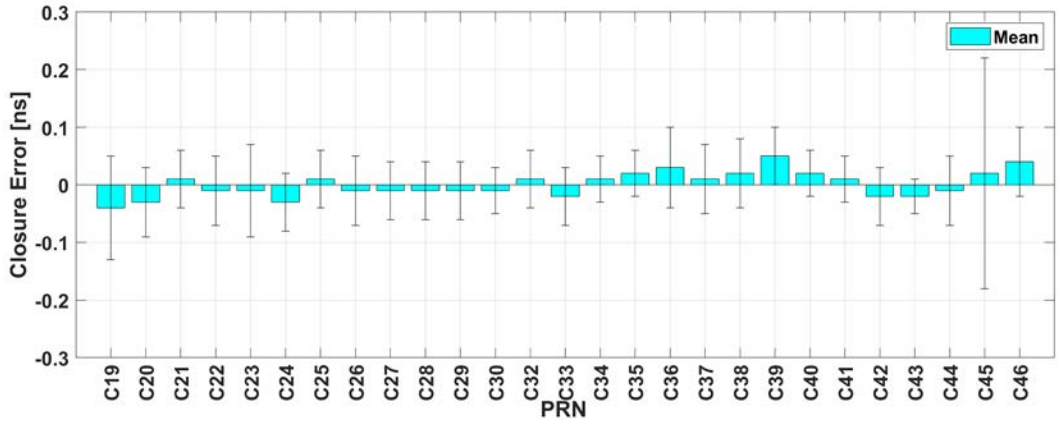

Figure 7 Mean values and STDs of closure error for the type of C1X-C2I-C5X

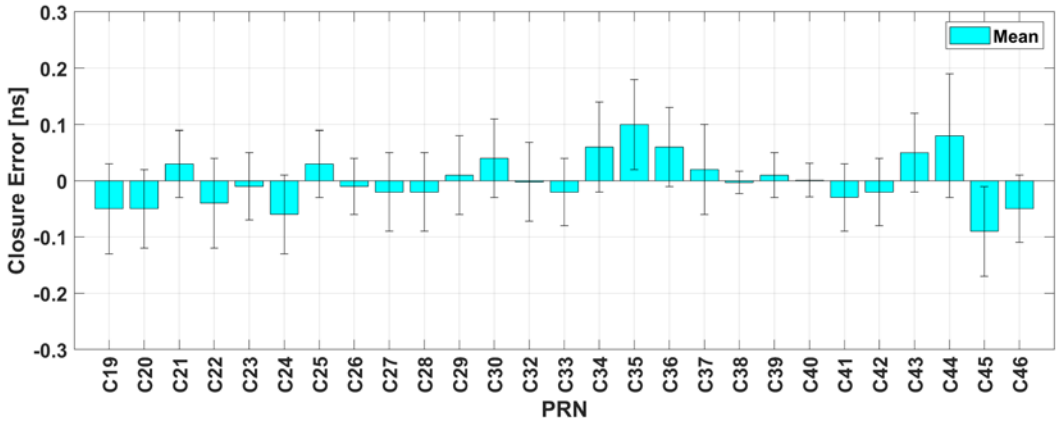

Figure 8 Mean values and STDs of closure error for the type of C1X-C5X-C6I

3.3 External consistency of the estimated BDS-3 DCBs

To further evaluate the external consistency of the estimated BDS-3 DCBs in this study (Hohai University, HHU), the DCB products of both DLR and CAS are used as references. Specifically, the DCB products of DLR and CAS are available at ftp.aiub.unibe.ch/CODE/ and ftp.gipp.org.cn/product/dcb/mgex/, respectively. For the common types of DCB products in HHU and the other two institutions, the deviation results can be obtained directly, which are defined as the directly estimated DCBs in this study. However, due to the limited DCB products provided by DLR and CAS, some estimated DCBs cannot be compared with the DCB products of DLR and CAS directly. Hence, the deviation results can be obtained by using the linear combinations of DCB products, which are defined as the DCB combinations in this study. Also, there may exist a datum transformation between the compared satellite sets [3]. The daily deviation series of the estimated DCBs for the types of C1P-C6I and C2I-C1X compared to CAS and DLR are depicted in Figures 9 to 10, respectively. It can be found that the accuracy of the estimated DCBs exhibits comparable performance compared to CAS and DLR, and the daily deviations for most satellites are within 0.2 ns. In addition, the monthly mean deviations of each satellite between HHU and the other two institutions are shown in Figures 11 to 14. It can be found that the mean deviations for each satellite between HHU and CAS are mainly within 0.3 ns, and the mean deviations for each satellite between HHU and DLR are mainly within 0.2 ns for the directly estimated DCB products. This verifies a good external consistency for the estimated BDS-3 DCBs in this study. Moreover, most mean deviations for each satellite between HHU and DCB combinations products of CAS and DLR are both within 0.6 ns. The accuracy of the directly estimated DCBs behave better than that of DCB combinations products, which further verifies the necessity to estimate the multi-frequency DCBs directly for BDS-3 satellites.

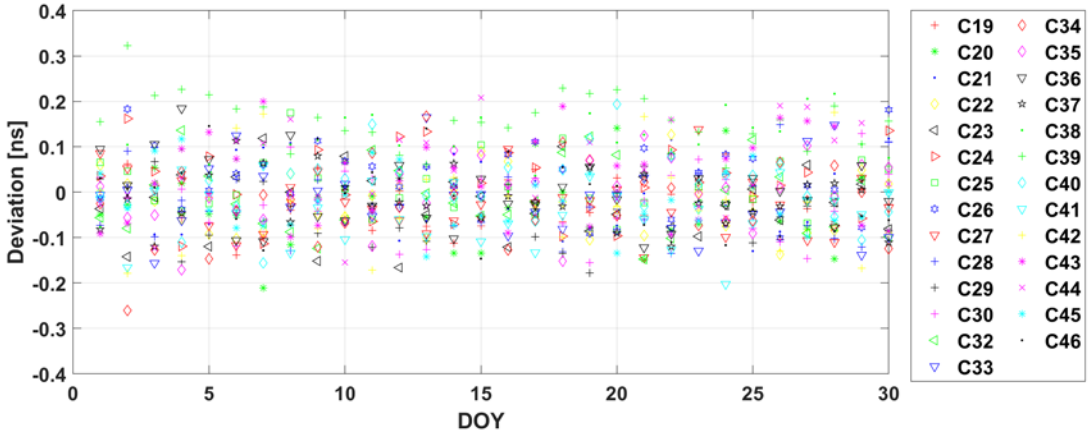

Figure 9 Daily deviation series of the estimated DCBs for the type of C1P-C6I

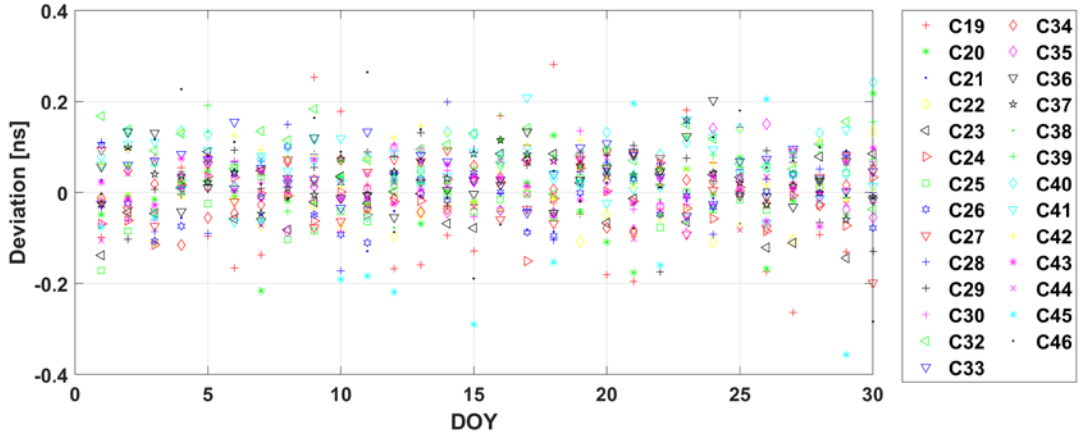

Figure 10 Daily deviation series of the estimated DCBs for the type of C2I-C1X

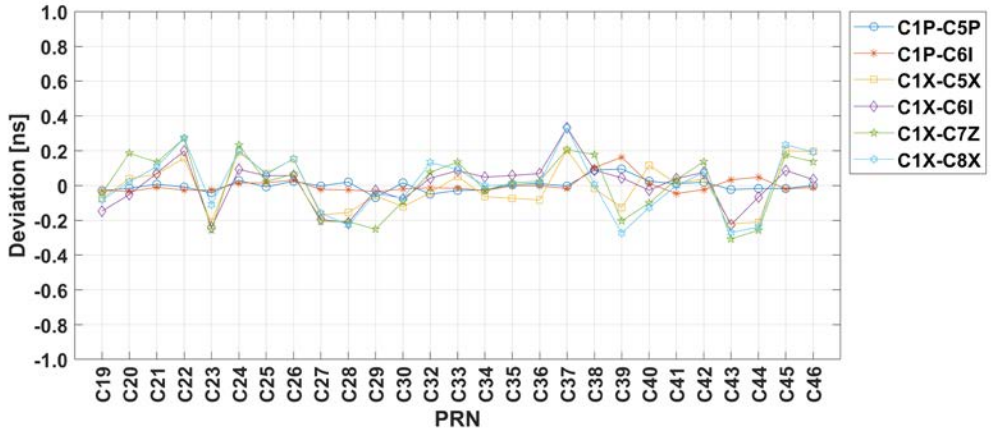

Figure 11 Mean deviations of each satellite for the directly estimated DCBs between HHU and CAS

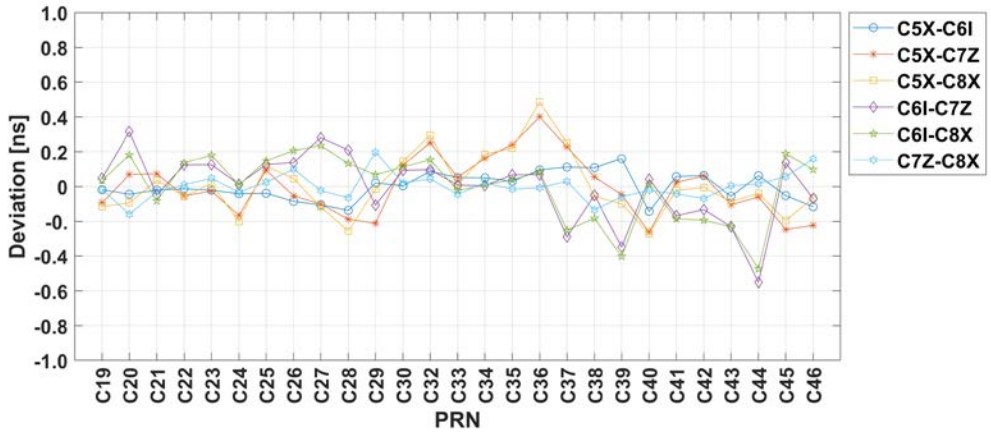

Figure 12 Mean deviations of each satellite for the DCB combinations between HHU and CAS

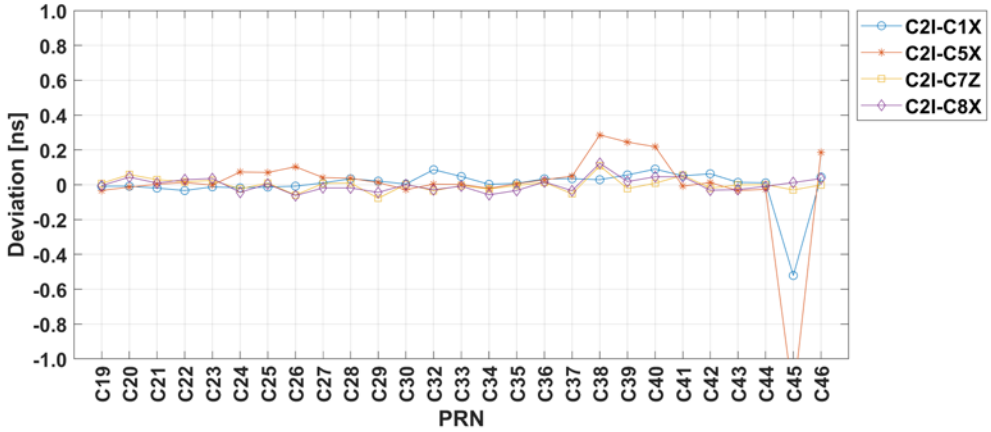

Figure 13 Mean deviations of each satellite for the directly estimated DCBs between HHU and DLR

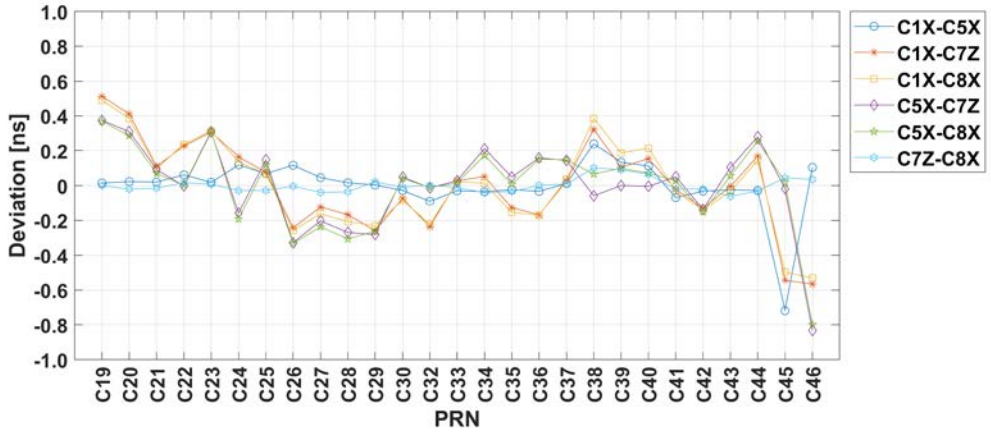

Figure 14 Mean deviations of each satellite for the DCB combinations between HHU and DLR

The monthly mean deviations of each satellite between HHU and the other two institutions are further listed in Tables 2 and 3 in detail. The HHU-CAS-1 denotes the mean deviations between the directly estimated DCBs of HHU and the DCB combinations products of CAS. The HHU-CAS-2 denotes the mean deviations between directly estimated DCBs of HHU and CAS. Similar definitions are used for HHU-DLR-1 and HHU-DLR-2, respectively. The bolded values are the mean deviations which are relatively large in the Tables. It can be found that the numbers of bolded values of HHU-CAS-1 and HHU-DLR-1 are significantly more than HHU-CAS-2 and HHU-DLR-2, respectively. Similar conclusions can be found in Figures 11 to 14, and this verifies the necessity to estimate the multi-frequency DCBs directly for BDS-3 satellites again.

Table 2 Monthly mean deviations of DCBs between HHU and CAS for each satellite (unit: ns)

PRN	HHU-CAS-1						HHU-CAS-2					
	C5XC6I	C5XC7Z	C5XC8X	C6IC7Z	C6IC8X	C7ZC8X	C1PC5P	C1PC6I	C1XC5X	C1XC6I	C1XC7Z	C1XC8X
C19	-0.02	-0.09	-0.12	0.05	0.03	-0.02	-0.03	-0.03	-0.07	-0.15	-0.04	-0.08
C20	-0.04	0.07	-0.09	**0.32**	0.18	-0.16	-0.02	-0.03	0.04	-0.05	0.18	0.02
C21	-0.02	0.07	0.04	-0.05	-0.08	-0.03	0.01	-0.01	0.06	0.07	0.13	0.11
C22	-0.01	-0.05	-0.06	0.12	0.14	0.01	0.01	-0.03	0.15	0.19	**0.27**	**0.27**
C23	-0.02	-0.03	0.02	0.12	0.18	0.05	-0.04	-0.03	-0.20	-0.20	**-0.25**	-0.11
C24	-0.04	-0.16	-0.20	0.01	0.01	-0.03	0.03	0.01	0.19	0.09	0.20	0.20
C25	-0.04	0.09	0.12	0.13	0.15	0.02	0.01	0.01	0.07	0.06	0.02	0.06
C26	-0.09	-0.05	0.04	0.14	**0.21**	0.10	0.02	0.03	0.15	0.06	0.06	0.15
C27	-0.11	-0.10	-0.12	**0.28**	**0.23**	-0.02	0.00	-0.02	-0.17	-0.19	-0.20	-0.16
C28	-0.14	-0.19	**-0.25**	**0.21**	0.13	-0.07	0.02	-0.03	-0.16	-0.20	-0.20	**-0.22**
C29	0.02	**-0.21**	-0.02	-0.11	0.07	0.20	-0.07	-0.04	-0.06	-0.03	**-0.25**	-0.05
C30	0.00	0.12	0.14	0.09	0.11	0.02	0.02	-0.02	-0.12	-0.08	-0.09	-0.07
C32	0.09	**0.25**	**0.29**	0.09	0.15	0.04	-0.05	-0.01	-0.04	0.04	0.07	0.13
C33	0.05	0.05	0.01	0.01	-0.02	-0.04	-0.03	-0.02	0.05	0.08	0.13	0.09
C34	0.05	0.16	0.19	0.01	0.01	0.02	-0.03	-0.03	-0.06	0.05	-0.02	-0.00
C35	0.03	**0.24**	**0.22**	0.07	0.04	-0.02	0.01	0.00	-0.07	0.06	0.01	0.01
C36	0.09	**0.40**	**0.49**	0.07	0.09	-0.01	0.01	0.00	-0.08	0.07	0.02	0.01
C37	0.11	**0.23**	**0.25**	**-0.29**	**-0.25**	0.03	0.00	-0.02	0.20	**0.30**	0.20	**0.34**
C38	0.11	0.06	-0.06	-0.05	-0.18	-0.13	0.09	0.10	-0.02	0.09	0.17	0.01
C39	0.16	-0.05	-0.10	**-0.35**	-0.40	-0.06	0.09	0.16	-0.13	0.04	-0.20	**-0.27**
C40	-0.14	**-0.26**	**-0.27**	0.04	0.01	-0.02	0.02	0.01	0.11	-0.03	-0.10	-0.12
C41	0.06	0.02	-0.02	-0.17	-0.19	-0.04	0.01	-0.05	0.01	0.04	0.03	-0.00
C42	0.06	0.06	-0.01	-0.13	-0.19	-0.07	0.02	-0.02	0.04	0.08	0.13	0.07
C43	-0.06	-0.10	-0.09	**-0.23**	**-0.23**	0.01	-0.02	0.03	-0.20	**-0.22**	**-0.31**	**-0.27**
C44	0.06	-0.06	-0.04	**-0.55**	**-0.47**	0.02	-0.02	0.05	-0.20	-0.07	**-0.25**	**-0.23**
C45	-0.05	**-0.25**	-0.19	0.14	0.19	0.06	-0.02	-0.02	0.20	0.09	0.17	**0.23**
C46	-0.12	**-0.22**	-0.06	-0.07	0.10	0.16	0.00	-0.01	0.19	0.03	0.13	0.19

3.4 Stability of the estimated BDS-3 DCBs

To further analyze the stability of the estimated DCBs for BDS-3 in this study, the daily series of the estimated DCBs for the types of C1P-C5P and C2I-C1X are depicted in Figures 15 to 16. It can be found that the daily DCB solutions for the type of C1P-C5P are between -40 ns~30 ns, and the daily DCB solutions for the type of C1P-C5P are between -6 ns~4 ns for all satellites. The daily DCB solutions for both two types exhibit good stability for each satellite. In addition, the monthly mean values of STDs for the estimated DCBs are listed in Table 4. The bolded values are the STDs of DCB combination products for DLR and CAS. It can be found that the monthly mean values of STDs for the estimated DCBs in this study are all smaller than 0.12 ns, which exhibits good stability. The differences of STDs between HHU and the other two institutions are within 0.02 ns, which further illustrates the consistency of stability between them. Besides, the STDs of the directly estimated DCBs for HHU are generally smaller than that of the DCB combination products for DLR and CAS. This also verifies the necessity to estimate the multi-frequency DCBs directly for BDS-3 satellites.

Table 3 Monthly mean deviations of DCBs between HHU and DLR for each satellite (unit: ns)

PRN	HHU-DLR-1						HHU-DLR-2			
	C1XC5X	C1XC7Z	C1XC8X	C5XC7Z	C5XC8X	C7ZC8X	C2IC1X	C2IC5X	C2IC7Z	C2IC8X
C19	0.01	**0.51**	**0.49**	**0.37**	**0.37**	0.00	-0.01	-0.03	0.01	0.00
C20	0.02	**0.41**	**0.39**	**0.31**	**0.29**	-0.02	-0.01	-0.01	0.06	0.04
C21	0.02	0.11	0.10	0.09	0.07	-0.02	-0.02	0.00	0.03	0.01
C22	0.06	**0.23**	**0.24**	0.00	0.00	0.02	-0.03	0.01	0.02	0.03
C23	0.02	**0.31**	**0.31**	**0.31**	**0.31**	0.01	-0.01	0.00	0.03	0.04
C24	0.12	0.16	0.13	-0.16	-0.19	-0.03	-0.02	0.07	-0.02	-0.04
C25	0.07	0.08	0.07	0.15	0.12	-0.03	-0.01	0.07	0.01	0.00
C26	0.12	**-0.24**	**-0.26**	**-0.33**	**-0.33**	0.00	-0.01	0.10	-0.06	-0.06
C27	0.04	-0.12	-0.16	-0.20	**-0.24**	-0.04	0.01	0.04	0.01	-0.02
C28	0.02	-0.17	**-0.21**	**-0.27**	**-0.31**	-0.04	0.03	0.04	0.01	-0.02
C29	0.00	**-0.26**	**-0.23**	**-0.28**	**-0.26**	0.02	0.02	0.01	-0.08	-0.04
C30	-0.03	-0.07	-0.08	0.05	0.04	-0.01	0.00	-0.03	0.00	0.00
C32	-0.09	**-0.24**	**-0.22**	-0.01	-0.01	0.00	0.09	0.00	-0.03	-0.03
C33	-0.03	0.03	0.02	0.03	0.01	-0.01	0.05	0.00	-0.01	-0.01
C34	-0.03	0.05	0.01	**0.21**	0.17	-0.04	0.00	-0.02	-0.02	-0.06
C35	-0.02	-0.13	-0.16	0.05	0.01	-0.03	0.01	0.01	0.00	-0.03
C36	-0.03	-0.17	-0.17	0.16	0.15	0.00	0.03	0.03	0.01	0.02
C37	0.01	0.03	0.04	0.14	0.15	0.01	0.03	0.05	-0.05	-0.03
C38	**0.24**	**0.32**	**0.39**	-0.06	0.07	0.10	0.03	**0.30**	0.11	0.12
C39	0.13	0.10	0.19	0.00	0.10	0.09	0.06	**0.24**	-0.02	0.02
C40	0.11	0.15	**0.21**	0.00	0.07	0.06	0.09	0.20	0.01	0.05
C41	-0.07	-0.02	-0.03	0.05	0.03	-0.02	0.05	-0.01	0.05	0.05
C42	-0.03	-0.13	-0.14	-0.14	-0.15	-0.02	0.06	0.01	-0.02	-0.03
C43	-0.02	0.00	-0.03	0.10	0.06	-0.06	0.01	-0.03	0.00	-0.03
C44	-0.03	0.17	0.14	**0.28**	**0.25**	-0.03	0.01	-0.03	0.00	-0.01
C45	**-0.72**	**-0.54**	**-0.50**	-0.02	0.02	0.04	**-0.50**	**-1.22**	-0.03	0.01
C46	0.10	**-0.57**	**-0.53**	**-0.83**	**-0. 80**	0.03	0.04	0.18	0.00	0.04

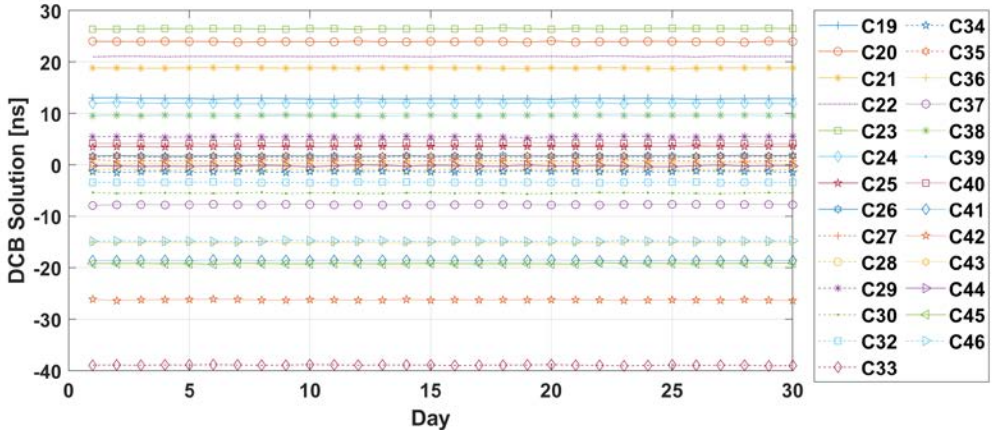

Figure 15 Daily solution series of the estimated DCB for the type of C1P-C5P

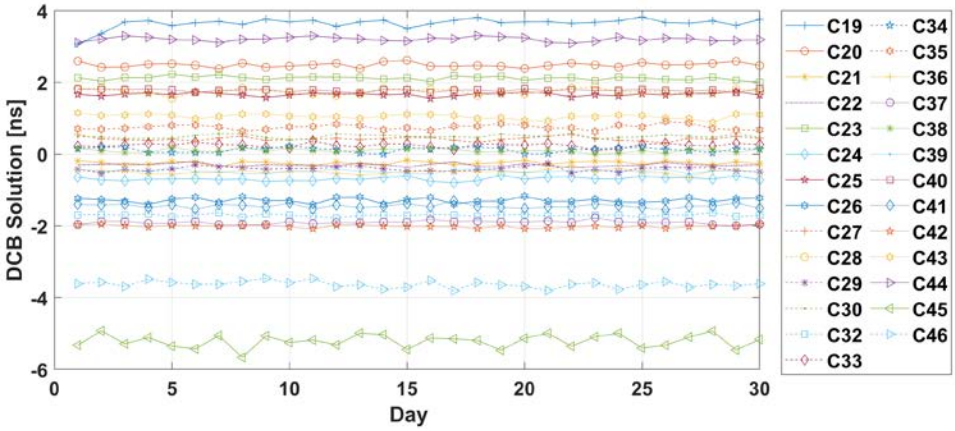

Figure 16 Daily solution series of the estimated DCB for the type of C2I-C1X

Table 4 Monthly mean values of STDs for the 19 types of the estimated DCBs (unit: ns)

Type	HHU	CAS	DLR
C1P-C2I	0.05	**0.06**	\
C1P-C5P	0.09	0.08	\
C1P-C6I	0.06	0.06	\
C1X-C5X	0.09	0.09	\
C1X-C6I	0.10	0.10	\
C1X-C7Z	0.11	0.09	\
C1X-C8X	0.11	0.10	\
C2I-C1X	0.06	**0.09**	0.07
C2I-C5X	0.11	**0.11**	0.12
C2I-C7Z	0.12	**0.10**	0.10
C2I-C8X	0.12	**0.12**	0.10
C5P-C2I	0.09	**0.08**	\
C5P-C6I	0.04	**0.05**	\
C5X-C6I	0.09	**0.10**	**0.11**
C5X-C7Z	0.05	**0.08**	**0.11**
C5X-C8X	0.03	**0.07**	**0.10**
C6I-C7Z	0.12	**0.14**	**0.11**
C6I-C8X	0.11	**0.11**	**0.11**
C7Z-C8X	0.03	**0.06**	**0.06**

4. Conclusions

In this paper, we focus on the estimation and analysis of BDS-3 multi-frequency differential code bias, especially for the new frequencies. The estimation method of BDS-3 multi-frequency DCBs is introduced first, and then the estimated DCBs in this study are carefully analyzed compared to the DCB products of both DLR and CAS in terms of inner consistency, external consistency, and stability.

For the results of inner consistency, most of these closure error series are within 0.2 ns, and the closure error series of each satellite fluctuate near zero and have no obvious systematic deviation. The monthly mean values of the closure errors for each satellite are within 0.2 ns, and most of them are within 0.1 ns. Hence, the inner consistency of the estimated BDS-3 DCBs in this study exhibits good performance. For the results of external consistency, the mean deviations for each satellite between HHU and CAS are mainly within 0.3 ns, and the mean deviations for each satellite between HHU and DLR are mainly within 0.2 ns for the directly estimated DCB products. This verifies a good external consistency for the estimated BDS-3 DCBs in this study. For the results of stability, the monthly mean values of STDs for the estimated BDS-3 DCBs are all smaller than 0.12 ns, which exhibits good stability. The differences of STDs between HHU and the other two institutions are within 0.02 ns, which illustrates their consistency of stability. The STDs of the directly estimated BDS-3 DCBs in this study are generally smaller than that of the DCB combination products of DLR and CAS. Therefore, the accuracy and stability of the directly estimated BDS-3 DCBs exhibit better performance than that of DCB combination products, which further verifies the necessity to estimate the multi-frequency DCBs directly for BDS-3 satellites.

Acknowledgment

This study was supported by The National Natural Science Foundation of China (41830110, 42004014), Natural Science Foundation of Jiangsu Province (BK20200530), Open Project Research Fund of Technology Innovation Center for Geological Environment Monitoring MNR (2022KFK1212002), China Postdoctoral Science Foundation

(2020M671324), Jiangsu Planned Projects for Postdoctoral Research Funds (2020Z412).

References

[1] M Hernández-Pajares, J.M. Juan, J. Sanz, R. Orus, A. Garcia-Rigo, J. Feltens, A. Komjathy, S.C. Schaer, A. Krankowski, The IGS VTEC maps: a reliable source of ionospheric information since 1998, J. Geod. 83 (2009) 263–275. https://doi.org/10.1007/s00190-008-0266-1.

[2] O. Montenbruck, A. Hauschild, Code biases in multi-GNSS point positioning, ION-ITM-2013, 2013.

[3] N. Wang, Y. Yuan, Z. Li, O. Montenbruck, B. Tan, Determination of differential code biases with multi-GNSS observations, J. Geod. 90 (2016) 209–228, doi.org/10.1007/s00190-015-0867-4.

[4] E., Sardón, A., Rius, N., Zarraoa, Estimation of the transmitter and receiver differential biases and the ionospheric total electron content from Global Positioning System observations, Radio Sci. (1994), doi.org/10.1029/94RS00449.

[5] Z. Li, Y. Yuan, L. Hui, J. Ou, X. Huo, Two-step method for the determination of the differential code biases of COMPASS satellites, J. Geod. 86 (2012) 1059–1076, doi.org/10.1007/s00190-012-0565-4.

[6] F. Guo, X. Zhang, J. Wang, Timing group delay and differential code bias corrections for BeiDou positioning, J. Geod. 89 (2015) 427–445, doi.org/10.1007/s00190-015-0788-2.

[7] B. Zhang, P. Teunissen, Y. Yuan, H. Zhang, M. Li, Joint estimation of vertical total electron content (VTEC) and satellite differential code biases (SDCBs) using low-cost receivers, J. Geod. 92 (2018) 401–413, doi.org/10.1007/s00190-017-1071-5.

[8] T. Liu, B. Zhang, Y. Yuan, M. Li, Real-Time Precise Point Positioning (RTPPP) with raw observations and its application in real-time regional ionospheric VTEC modeling, J. Geod. 92 (2018) 1–17, doi.org/10.1007/s00190-018-1118-2.

[9] A.J. Mannucci, BD Wilson, D.N. Yuan, C.H. Ho, U.J. Lindqwister, T.F. Runge, A global mapping technique for GPS-derived ionospheric total electron content measurements, Radio Sci. 33 (1998) 565–582, doi.org/10.1029/97RS02707.

[10] A. Krankowski, I.I. Shagimuratov, I.I. Ephishov, A. Krypiak-Gregorczyk, G. Yakimova, The occurrence of the mid-latitude ionospheric trough in GPS-TEC measurements, Adv. Space Res. 43 (2009) 1721–1731, doi.org/10.1016/j.asr.2008.05.014.

[11] O. Montenbruck, A. Hauschild, P. Steigenberger, Differential Code Bias Estimation using Multi-GNSS Observations and Global Ionosphere Maps, NAVIGATION. 61 (2014) 191–201. doi.org/10.1002/navi.64.

[12] W. Li, M. Li, C. Shi, R. Fang, W. Bai, GPS and BeiDou Differential Code Bias Estimation Using Fengyun-3C Satellite Onboard GNSS Observations, Remote Sens. 9 (2017) 1239, doi.org/10.3390/rs9121239.

[13] Y. Zhu, S. Tan, L. Feng, X. Cui, X. Jia, Estimation of the DCB for the BDS-3 New Signals Based on BDGIM Constraints, Adv. Space Res. (2020). doi.org/10.1016/j.asr.2020.05.019.

[14] J. Lin, X. Yue, S. Zhao, Estimation and analysis of GPS satellite DCB based on LEO observations, GPS Solut. (2016), doi.org/10.1007/s10291-014-0433-1.

[15] L. Yuan, S. Jin, M.M. Hoque, Estimation of LEO-GPS receiver differential code bias based on inequality constrained least square and multi-layer mapping function, GPS Solut. 24 (2020). https://doi.org/10.1007/s10291-020-0970-8.

[16] L. Yuan, M. Hoque, S. Jin, A new method to estimate GPS satellite and receiver differential code biases using a network of LEO satellites, GPS Solut. 25 (2021) 1–12. doi.org/10.1007/s10291-021-01109-y.

[17] X. Li, T. Ma, W. Xie, K. Zhang, J. Huang, X. Ren, FY-3D and FY-3C onboard observations for differential code biases estimation, GPS Solut. 23 (2019), doi.org/10.1007/s10291-019-0850-2.

[18] X. Li, W. Zhang, K. Zhang, Q. Zhang, Y. Yuan, GPS satellite differential code bias estimation with current eleven low earth orbit satellites, J. Geod. 95 (2021), doi.org/10.1007/s00190-021-01536-2.

[19] R. Jin, S. Jin, G. Feng, M_DCB: Matlab code for estimating GNSS satellite and receiver differential code biases, Gps Solut. 16 (2012) 541–548. doi.org/10.1007/s10291-012-0279-3.

[20] B. Shu, H. Liu, L. Xu, X. Gong, R. Zhang, Analysis of satellite-induced factors affecting the accuracy of the BDS satellite differential code bias, GPS Solut. (2016) 1–12. doi.org/10.1007/s10291-016-0577-2.

[21] X. Li, W. Xie, J. Huang, T. Ma, X. Zhang, Y. Yuan, Estimation and analysis of differential code biases for BDS3/BDS2 using iGMAS and MGEX observations, J. Geod. 93 (2019) 419–435. doi.org/10.1007/s00190-018-1170-y.

[22] Y. Yang, Y. Mao, B. Sun, Basic performance and future developments of BeiDou global navigation satellite system, Satell. Navig. 1 (2020) 1, doi.org/10.1186/s43020-019-0006-0.

[23] Y. Yang, X.U. Yangyin, L.I. Jinlong, C. Yang, Progress and performance evaluation of BeiDou global navigation satellite system: Data analysis based on BDS-3 demonstration system, Sci. China Earth Sci. 61 (2018) 614–624. doi.org/10.1007/s11430-017-9186-9.

[24] J. Sanz, J. Miguel Juan, A. Rovira-Garcia, G. González-Casado, GPS differential code biases determination: methodology and analysis, GPS Solut. 21 (2017) 1549–1561, doi.org/10.1007/s10291-017-0634-5.

Authors

Haijun Yuan received the M.S. degree from Hohai University, Nanjing, China in 2021. He is currently a Ph.D candidate at the School of Earth Sciences and Engineering, Hohai University. His current research mainly focuses on multi-frequency and multi-constellation GNSS precise positioning and navigation.

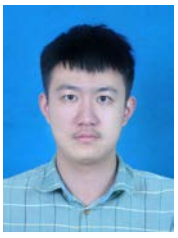

Zhuoming Hu received the M.S. degree from Hohai University, Nanjing, China in 2022. His research interests include the GNSS data processing, real-time precise positioning and navigation.

Xiufeng He received the Ph.D. degree from the Hong Kong Polytechnic University in 1998. She is currently a professor at the School of Earth Sciences and Engineering, Hohai University, Nanjing, China. Her research interests include satellite geodesy, deformation monitoring, multi-source data fusion, and integrated navigation.

Zhetao Zhang received the Ph.D. degree from Tongji University, Shanghai, China in 2019. He is currently an associate professor at the School of Earth Sciences and Engineering, Hohai University, Nanjing, China. His current research focuses on the GNSS precise positioning and navigation under the conditions including canyon environment, low-cost receiver, and multi-GNSS situation.